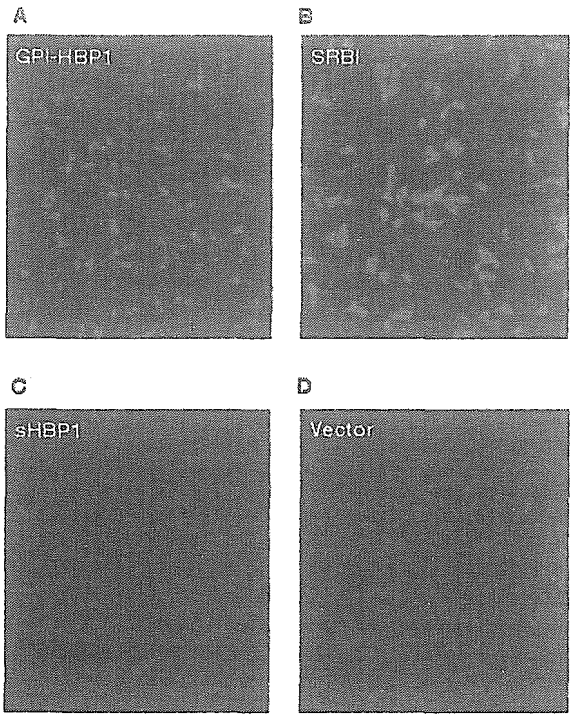

FIG. 1. **Visualization of receptor mediated uptake of fluorescent HDL by CHO cells expressing murine GPI-HBP1.** Transiently expressing cells were used in this study. Murine GPI-HBP1 cDNA (pHRC7) (*A*), murine SRBI cDNA (*B*), murine sHBP1 cDNA (*C*), and parental vector (pZeoSV2) (*D*) were independently introduced into LDL receptor-deficient ldlA7 cells as described under "Experimental Procedures." After a 2-h incubation with DiI-HDL at 37 °C, the cells were washed and fixed, and the presence of fluorescent DiI in the fixed cell was detected under fluorescent microscopy.

```
GPI-HBP1    MKALRAVLLILLLSGQPGSGHAQEDGDADPEPENYNYDDDDDEEEEETNMIPGSRDRAP  60
sHBP1       ************************************D*****************        60

GPI-HBP1    LQCVFCQVLHSGESCNQTQSCSSGKPFCITLVSHSGTDKGYLTTYSMWCTDTCQPIIKTV 120
sHBP1       ***********************************ASSLVCGRQGPEDPFSSNQDALA 120

GPI-HBP1    GGTQMTQTCCQSTLCNIPPHQNPQVQNPLGGRADSPLESGTRHPQGGKPSHPQVVKAAHP 180
sHBP1       SPS                                                         123

GPI-HBP1    QSDGANLPKSGKANQPQGSGAGYPSGWTKPGNIALLLSFFTCLWASGA            228
```

FIG. 2. **Amino acid sequence of murine GPI-HBP1.** The amino acid sequence of murine GPI-HBP1 deduced from the cDNA is compared with that of murine sHBP1. Identical amino acids are indicated by *asterisks*. The N- and C-terminal hydrophobic amino acids were *boxed*. A cluster of negatively charged amino acids is *underlined*. The Ly-6 motif is indicated by a *dotted underline*.

EXPERIMENTAL PROCEDURES

Materials—Human HDL, LDL, acetylated LDL and oxidized LDL, and newborn calf lipoprotein-deficient sera were prepared essentially as described previously (2, 11). ^{125}I-Labeled HDL was prepared according to the procedure as described previously (12). Oxidized LDL was prepared by dialyzing 1 ml of LDL (4–10 mg/ml) (prepared without β-hydroxytoluene) against saline solution containing 5 μM Cu_2SO_4 (2 × 500 ml) for 24–48 h at 4 °C. 1,1′-Dioctadecyl-3,3,3,3′-tetramethylindocarbocyanine perchlorate (DiI) was obtained from Molecular Probes (Eugene, OR) and was used to prepare fluorescent-labeled HDL as described previously (13). Human apoAI and AII, phosphatidylinositol-specific phospholipase C (*Bacillus cereus*, specific activity of 7.1 units/mg), egg yolk phosphatidylcholine, and brain phosphatidylserine were from Sigma. Phospholipid liposomes were prepared by extrusion through polycarbonate membranes as described previously (14): phosphatidylcholine liposomes (phosphatidylcholine/free-cholesterol, molar ratio 2:1) and phosphatidylserine liposomes (phosphatidylcholine/phosphatidylserine/free-cholesterol, molar ratio 1:1:1).

Standard Procedures—Standard molecular biology techniques were performed essentially as described by Sambrook and Russell (15). cDNA clones were subcloned into pBluescript vectors and sequenced by the dideoxy chain termination method with a BigDye Terminator Cycle Sequencing Ready Reaction kit (PE Biosystems) and a DNA sequencer (model 310, PE Biosystems). To analyze RNA in murine tissues, commercially available Northern blots (Clontech laboratories) were used for Northern blot analysis. ^{32}P-Labeled probes were prepared by priming with random hexanucleotides.

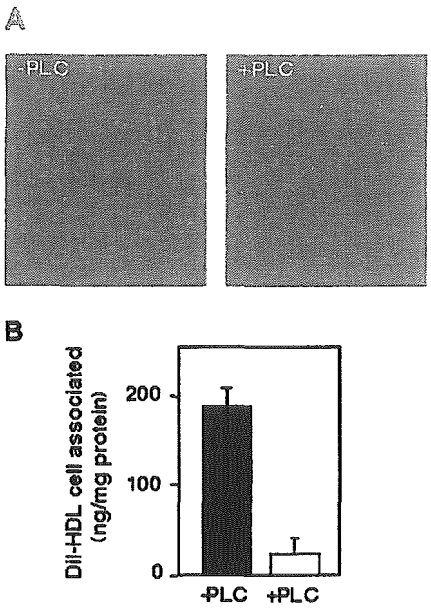

FIG. 3. **Effect of PIPLC treatment on DiI-HDL uptake.** *A*, murine GPI-HBP1 was transiently expressed in ldlA7 cells as described under "Experimental Procedures." After a 1-h incubation with or without PIPLC at 37 °C, cells were washed and incubated for the measurement of DiI-HDL uptake. *B*, DiI-HDL uptake. The amount of cell-associated DiI was determined as described under "Experimental Procedures." Values are the average of triplicate determinations, and *error bars* represent the range of the three measurements.

Expression Cloning—A cDNA library was constructed from poly(A) RNA isolated from the livers of LDL receptor-deficient male mice (16) in the pZeoSV2 vector (Invitrogen) using a *Not*I unidirectional primer. The cDNA library consisted with ~3 × 10^5 clones, and these clones were divided into small pools (300 clones/pool). Plasmid DNA from each pool was prepared using the QIAprep 96 Turbo Miniprep kit (Qiagen). On day 0, LDL receptor-lacking Chinese ovary cells, ldlA7 (17), were plated into 96-well plates (5 × 10^4/well) in minimum essential medium α supplemented with 10% fetal bovine serum, 100 units/ml penicillin, and 100 μg/ml streptomycin (medium A). On day 1, the cells in each plate were transfected with 0.1 μg of a cDNA pool using Effectene transfection reagent (Qiagen) according to the manufacturer's protocol. After incubation for 16 h, the transfection mixture was replaced with medium A. On day 3, the monolayers were refed with minimum essential medium α containing 2 μg/ml protein of DiI-HDL and 5% lipoprotein-deficient serum. After a 2-h incubation at 37 °C, the plates were washed twice with PBS containing 10 mg/ml BSA and then twice with PBS, and the cells were fixed with 3% formaldehyde in PBS for 15 min at room temperature. The presence of DiI in the fixed cell was detected by visual inspection under fluorescent microscopy. Positive pools were serially subdivided and retested to obtain positive cDNA clones.

Cell Culture and Transfection—The entire coding regions of murine GPI-HBP1 and SRBI were subcloned into the pRC/CMV vector (Invitrogen) for stable transfection. CHO ldlA7 cells were transfected with the expression plasmid using the LipofectAMINE reagent (Invitrogen) according to the manufacturer's instructions. Stably transfected cells were selected in Ham's F-12 medium containing 50 units/ml penicillin, 50 μg/ml streptomycin, and 2 mM glutamine (medium B) supplemented with 5% fetal bovine serum and 250 μg/ml G418 for 2 weeks. For ^{125}I-HDL and DiI-HDL binding studies and [^{3}H]cholesterol efflux assays (see below), cells were plated in 6-well (250,000 cells/well) dishes in medium B supplemented with 5% newborn calf lipoprotein-deficient serum and cultured for 48 h.

Phosphatidylinositol-specific Phospholipase C (PIPLC) Treatment—GPI-HBP1-expressing cells were incubated for 1 h in medium B supplemented with 5% newborn calf lipoprotein-deficient serum with or

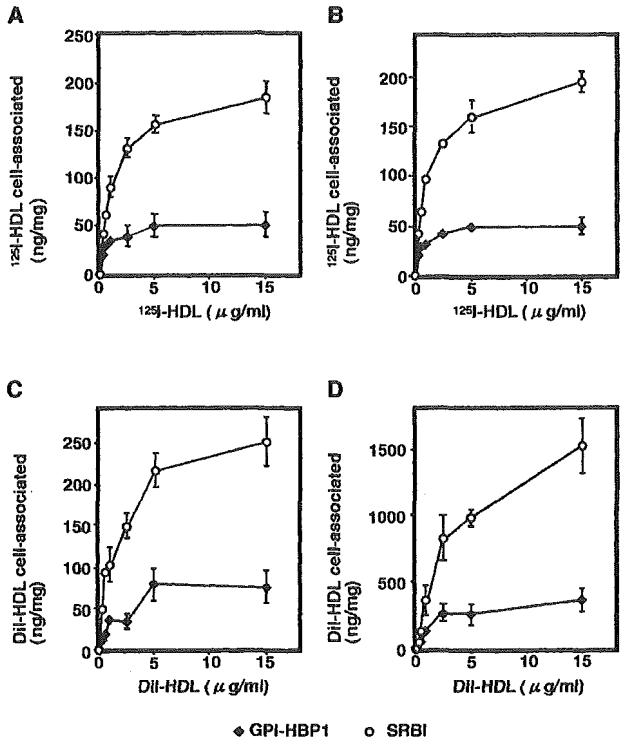

FIG. 4. **Concentration dependence of HDL binding to and HDL lipid uptake by GPI-HBP1 and SRBI-expressing cells.** CHO ldlA7 cells were stably transfected with expression vectors for murine GPI-HBP1, murine SRBI, or the control ("parental") vector (pRC/CMV) as described under "Experimental Procedures." Cells were plated in six-well dishes and incubated with the indicated amounts of either ^{125}I-HDL (*A* and *B*) or DiI-HDL (*C* and *D*) at either 4 °C (*A* and *C*) or 37 °C for 2 h. The amounts of specific ^{125}I-HDL binding or DiI uptake (spectrofluorimetry) were determined by subtracting the values obtained with parental vector (pRC/CMV) transfected cells from those obtained with a given expression plasmid as described under "Experimental Procedures." Similar results have been observed in multiple independent experiments, and the data shown are representative. *Error bars* represent the range of variations in the triplicate determinations.

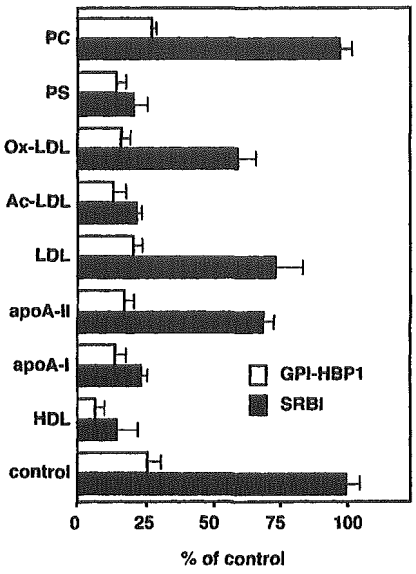

FIG. 5. **Inhibition of ^{125}I-HDL binding to GPI-HBP1 expressing cells by various compounds.** GPI-HBP1 or SRBI expressing cells were incubated with 10 μg/ml ^{125}I-HDL at 4 °C for 2 h in the presence of 200 μg/ml of the indicated compound. *PC*, phosphatidylcholine; *PS*, phosphatidylserine; *Ox-LDL*, oxidized LDL; *Ac-LDL*, acetylated LDL. The 100% control values for the binding ^{125}I-HDL (in the absence of inhibitors) of GPI-HBP1- and SRBI-expressing cells were 48.9 and 190 ng/mg protein, respectively. *Error bars* represent the range of variations in the triplicate determinations.

without 1 unit/ml PIPLC. Cells were then washed and incubated for the measurement of DiI-HDL uptake.

^{125}I-HDL-binding and Association Assays—Cells were washed once with medium B and then refed with medium B containing 0.5% (w/v) fatty acid-free BSA and the indicated concentrations of ^{125}I-HDL. After a 2-h incubation at 37 °C, cells were washed once with 50 mM Tris-HCl, pH 7.4, and 0.15 M NaCl (buffer A) containing 2 mg/ml BSA followed by two quick washes with buffer A without BSA. Cells were then solubilized with 0.1 N NaOH for 30 min at room temperature on a shaker, and we determined the amounts of cell-associated radioactivity using a γ-counter. The protein content was determined using the method of Lowry *et al.* (18). For 4 °C binding studies, the protocol was identical to that at 37 °C with the exception that the cells were prechilled on ice for 15 min and incubated with ^{125}I-HDL at 4 °C for 2 h. Specific cell association or binding was determined by subtracting the values obtained with parental vector (pRC/CMV) transfected cells from those obtained with a given expression plasmid.

Fluorimetric Assay of DiI-HDL Uptake—DiI-HDL was used to measure the cellular association and uptake of fluorescence by cells stably expressing GPI-HBP1 or SRBI according to the procedure as described by Acton *et al.* (3). Cells were washed once with medium B and then refed with medium B containing 0.5% (w/v) fatty acid-free BSA and the indicated concentrations of DiI-HDL. After incubation at 37 °C for 2 h, cells were washed twice with PBS containing 5 mM $CaCl_2$ and 5 mM $MgCl_2$ (5 min/wash). Cell-associated DiI was then solubilized in 0.5 ml of Me_2SO at room temperature for 2 h, and the fluorescence was measured using a spectrofluorimeter. The amount of DiI in each sample expressed as equivalent amounts of DiI-HDL (micrograms of protein) was calculated by comparing the fluorescence intensity of the sample to that from a standard curve generated by dissolving DiI-HDL in Me_2SO. Specific DiI uptake was determined by subtracting the values obtained with parental vector transfected cells from those obtained with a given expression plasmid.

[^{3}H]Cholesterol Efflux from Stably Transfected CHO ldlA7 Cells—HDL-dependent cholesterol efflux study was performed according to the procedure described by Gu *et al.* (19). Cells (~70% confluent) were incubated for 48 h with 0.2 μCi/ml [1,2-^{3}H]cholesterol (40–60 Ci/mmol, Amersham Biosciences). After washing five times with PBS containing 1% fatty acid-free BSA, radiolabeled cells were incubated overnight in Ham's F12 containing 1% fatty acid-free BSA to allow for the equilibration of cellular cholesterol pools. Cells were then washed and incubated for the indicated times in efflux medium (Ham's F12, 0.5% fatty acid-free BSA) with or without 40 μg/ml HDL. The efflux medium was collected and clarified by centrifugation for 1 min with a Microcentrifuge, and the radioactivity of each supernatant was determined by liquid scintillation counting. Cells were solubilized with 1% Triton X-100 in PBS for 30 min at room temperature, and the amount of [^{3}H]cholesterol in each lysate was determined. Total cellular [^{3}H]cholesterol was calculated as the sum of the radioactivity in the efflux medium plus the radioactivity in the cells and was used to calculate the [^{3}H]cholesterol efflux (percent of total [^{3}H]cholesterol released into the medium).

In Situ Hybridization—Digoxigenin-11-UTP-labeled single-stranded RNA probes were prepared with a digoxin/RNA-labeling mixture and the corresponding T3 or T7 RNA polymerase (Roche Molecular Biochemicals) according to the manufacturer's instructions. The entire coding region of murine GPI-HBP1 cDNA was subcloned into the pBluescript II vector (Stratagene) and used to prepare single-stranded RNA probes. Tissues from a C57BL/6J male mouse (10-weeks old) were fixed in PBS containing 4% paraformaldehyde at 4 °C for 12 h, dehydrated, and embedded in paraffin using a standard procedure. *In situ* hybridization was performed using 6-μm thick sections mounted on silane-coated glass slides. After digestion with 10 mg/ml proteinase K at 37 °C for 20 min, the tissue sections were hybridized with antisense or sense RNA probes at 50 °C for 16 h. For the reaction with antidigoxigenin antibodies, slides were washed with 100 mM Tris-HCl, pH 7.5 and 150 mM NaCl (buffer B), treated with 0.5% blocking reagent (Roche Molecular Biochemicals) in buffer B, and then incubated with alkaline phosphatase-coupled antidigoxigenin antibodies (diluted 1:750 in buffer B, Roche Molecular Biochemicals) for 1 h.

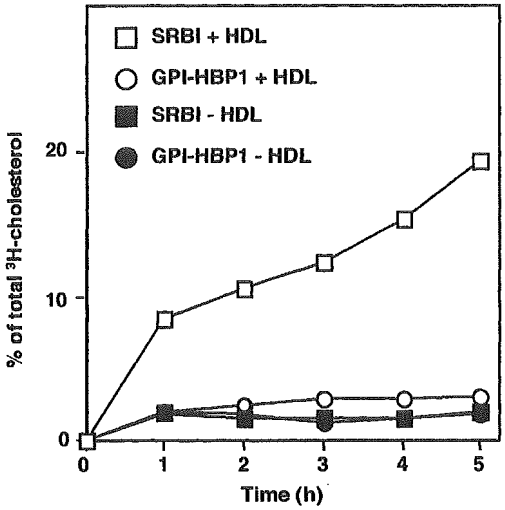

FIG. 6. **Lack of HDL-dependent cholesterol efflux in GPI-HBP1-expressing cells.** ldlA7 cells stably expressing GPI-HBP1 or SRBI were prelabeled with [^{3}H]cholesterol as described under "Experimental Procedures." Cells were incubated for the indicated times in medium containing 0.5% BSA with or without 40 μg/ml HDL. Results are expressed as percentages of radioactivities released in the culture media of the total radioactivities in media and cells. Values are the average of triplicate determinations. The *error bars* are too small to show.

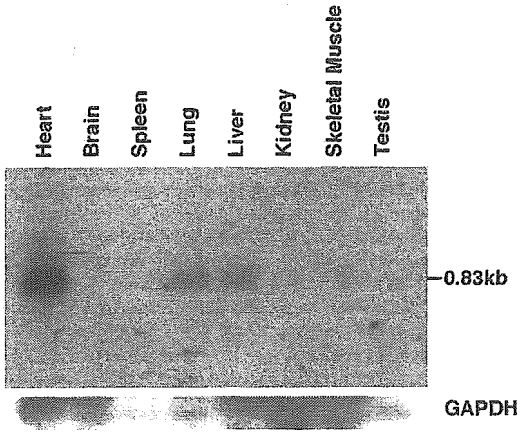

FIG. 7. **Tissue expression of GPI-HBP transcripts.** 2 μg of poly(A) RNA from the indicated murine tissues was probed with ^{32}P-labeled murine GPI-HBP1 (*upper panel*). The filters were exposed to Kodak X-Omat AR film with an intensifying screen at −80 °C for 48 h. The same samples were subsequently hybridized with a control probe for mouse glyceraldehyde-3-phosphate dehydrogenase (*GAPDH*) (*lower panel*) and exposed to Kodak X-Omat AR with an intensifying screen at −80 °C for 6 h.

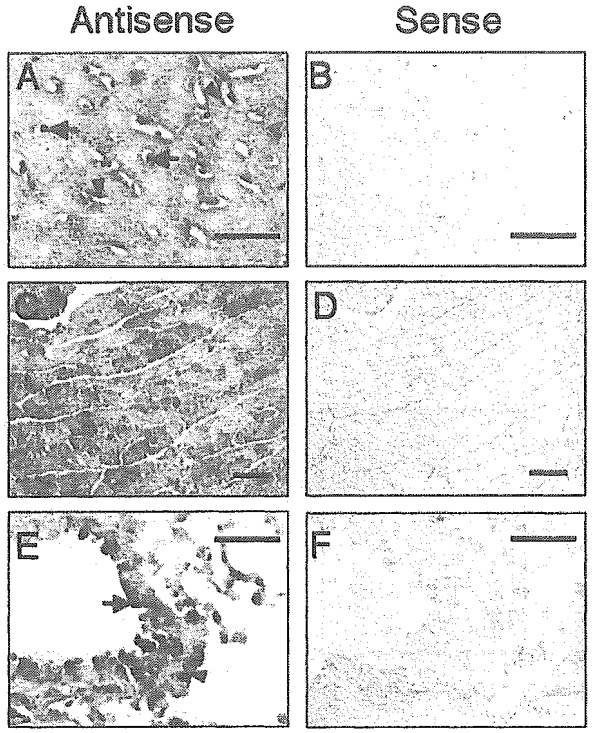

FIG. 8. ***In situ* hybridization analysis of GPI-HBP1 transcripts in mouse.** *Sections A, C,* and *E* were hybridized with an antisense probe to murine GPI-HBP1. *Sections B, D,* and *F* are negative controls with a sense probe. Hybridization signals were visualized in *blue*. Tissue sections prepared from liver (*A* and *B*), heart (*C* and *D*), and lung (*E* and *F*) of a normal male mouse were analyzed by *in situ* hybridization as described under "Experimental Procedures." GPI-HBP1 transcripts are localized in the Kupffer cells (indicated by *arrows* in *A*) and sinusoidal endothelium (*arrowheads* in *A*), but no significant accumulation is detected in the parenchymal cells. In the heart, the hybridization signal is detected in cardiac muscle cells (*C*). The intense hybridization signals are seen in bronchial epithelium (*arrow* in *E*) and alveolar macrophages (*arrowhead* in *E*) in the lung. *Bars*, 50 μm

RESULTS AND DISCUSSION

Expression Cloning of HDL-binding Proteins—We screened a cDNA library from murine liver for cDNAs that facilitate the binding of HDL when transiently expressed in LDL receptor-lacking ldlA7 cells. After screening a total of 960 pools of ~300 cDNA each, we obtained two pools of cDNAs that stimulated HDL binding to levels that were significantly higher than background. We then plated a total of 960 colonies from two positive pools into individual wells of 96-well plates. We prepared cDNAs from the pooled rows and columns of the plates. Four of these pools gave positive results. We then assayed individual clones from the wells at the intersections of the positive rows and columns and obtained two positive clones (Fig. 1). Nucleotide sequencing of these clones and subsequent BLAST search revealed that one corresponds to murine SRBI cDNA (3) and the other (designated pHRC7) encoded a protein of 228 amino acids (Fig. 2).

Structure of a GPI-anchored HDL-binding Protein—A hydropathy plot of the deduced amino acid sequence of the cDNA shows the presence of two hydrophobic regions (Fig. 2), one at the N terminus and the other at the C terminus. The former corresponds to a classical signal sequence of probable 19 amino acids in length, whereas the latter strongly resembles the hydrophobic region of GPI-anchored cell surface proteins. Excluding the N-terminal 19 amino acids, the mature protein would then consist of 209 amino acids with a calculated M_r of 22,603. This value is greatly smaller than those values of the previously characterized candidate receptors for HDL (4–8).

The predicted amino acid sequence revealed the presence of a region highly enriched with acidic amino acids (aspartate and glutamate) and a region similar to a highly conserved domain termed Ly-6 motif, which occurs singly in the GPI-anchored lymphoid differentiation antigen Ly-6 family, and is repeated 3-fold in urokinase-type plasminogen activator receptor. These results predicted that the cloned protein consists of an N-terminal signal sequence, an acidic region with a cluster of aspartate and glutamate residues, an Ly-6 motif, and a C-terminal hydrophobic region.

Based on the structural similarity with the GPI-anchored Ly-6 family proteins, we analyzed the effects of phosphatidylinositol-specific PIPLC treatment on the HDL binding. As shown in Fig. 3, the PIPLC treatment almost completely abol-

ished the uptake of DiI-HDL, suggesting that the cloned protein is indeed GPI-anchored. Therefore, we designate the cloned HDL-binding protein as GPI-HBP1.

EST data base search identified an isoform lacking the C-terminal half of GPI-HBP1. This isoform (designated sHBP1) shares the N-terminal signal sequence, the acidic region, and part of the Ly-6 motif with GPI-HBP1 but lacks the C-terminal hydrophobic region, suggesting that the isoform is a secreted form generated by alternative splicing. Consistent with the deduced structural feature, ldlA7 cells transiently transfected with sHBP1 failed to bind DiI-HDL on the cell surface (Fig. 1*C*).

BLAST searches of the GenBank™ databases revealed that GPI-HBP1 is structurally related to Ly-6 molecules, a set of GPI-anchored cell surface proteins belonging within a superfamily that includes the urokinase-type plasminogen activator receptor, the complement inhibitor CD59, the sperm antigen SP10, and more distantly, the snake venom neurotoxin family. The Ly-6 motif consists of ~90 amino acids with ten highly conserved cysteine residues (20). A comparison of the sequence of the Ly-6 motif in GPI-HBP1 with those in the Ly-6 family members revealed that these cysteine residues are completely conserved in the Ly-6 motif of GPI-HBP1 (data not shown). The phylogenetic tree of the Ly-6 family proteins of various origins indicates that GPI-HBP1 is most closely related to Ly-6 molecules (data not shown).

HDL Binding—To characterize lipoprotein-binding properties, cDNAs encoding GPI-HBP1 and SRBI were stably expressed in ldlA7 cells. The binding of ^{125}I (^{125}I-HDL) or fluorescent (DiI-HDL) labeled HDL was measured following incubation of the cells. As shown in Fig. 4, *A* and *B*, the saturation binding of ^{125}I-HDL was observed in both GPI-HBP1- and SRBI-expressing cells at 4 and 37 °C. Although the maximal binding of ^{125}I-HDL in GPI-HBP1-expressing cells was 3-fold lower than that of SRBI-expressing cells, the calculated K_d values of the two proteins were within the same range (2–3 μg/ml). The relative maximal binding activity between SRBI and GPI-HBP1 could not be determined because the expression levels of these two proteins in ldlA7 cells were unknown. Similar saturation binding was observed when cells were incubated with DiI-HDL at 4 °C (Fig. 4*C*). In contrast, when GPI-HBP1-expressing cells were incubated with DiI-HDL at 37 °C, the amounts of DiI-HDL binding by the cells were ~3-fold higher than those at 4 °C and unsaturable (Fig. 4*D*). Similarly, the amounts of DiI-HDL binding at 37 °C by SRBI-expressing cells were ~6-fold higher than those at 4 °C. Furthermore, compared with ^{125}I-HDL binding, the degradation of ^{125}I-HDL (trichloroacetic acid-soluble ^{125}I) at 37 °C was almost negligible in both cells (data not shown). These data indicate that GPI-HBP1, similar to SRBI (3), mediates selective lipid uptake but not the protein component of HDL.

Effects of SRBI Ligands—We next analyzed the effects of various ligands for SRBI (2, 14) on the binding of ^{125}I-HDL to GPI-HBP1-expressing cells. As shown in Fig. 5, in the presence of excess unlabeled HDL, the binding of ^{125}I-HDL to GPI-HBP1- and SRBI-expressing cells was strongly reduced. Compared with the strong inhibition of ^{125}I-HDL binding to SRBI-expressing cells by human apoAI (free form), phosphatidylserine, and acetylated LDL (inhibited by ~75%), the inhibitory effects by these compounds were relatively lower in GPI-HBP1-expressing cells (reduced by ~50%). Oxidized LDL, native LDL, and human apoAII had relatively weak inhibitory effects on ^{125}I-HDL binding to GPI-HBP1- and SRBI-expressing cells. These data show that HDL is bound to GPI-HBP1 most preferentially among various SRBI ligands including HDL, phosphatidylserine, and acetylated LDL.

Cholesterol Efflux—In addition to selective lipid uptake from HDL particles, SRBI mediates HDL-dependent cholesterol efflux. To test whether GPI-HBP1 also mediates cholesterol efflux, the cells were labeled with [^{3}H]cholesterol, allowed for the equilibration of cellular cholesterol pools, and then incubated with or without HDL. As shown in Fig. 6, SRBI-expressing cells exhibited HDL-dependent cholesterol efflux with time-dependent manner, whereas almost no cholesterol efflux was seen in GPI-HBP1-expressing cells in the absence or the presence of HDL. The lack of cholesterol efflux in GPI-HBP1 cells indicates that GPI-HBP1 mediates selective lipid uptake only, whereas SRBI mediates both influx and efflux of cholesterol.

Expression of GPI-HBP1 Transcripts—Northern blot analysis of RNA from various murine tissues revealed hybridization of the HBP1 probe to a major transcript of 0.8 kilobases with the highest expression in heart and, to a much lesser extent, in lung and liver (Fig. 7). Apparently, no transcripts were detected in other tissues including brain, kidney, skeletal muscle, spleen, and testis.

To locate cells expressing GPI-HBP1 transcripts, *in situ* hybridization was performed using tissue sections from murine liver, heart, and lung. In the liver, the accumulation of hybridization signals for GPI-HBP1 transcripts appearing dark blue were detected most intensely in the Kupffer cells and sinusoidal endothelium, but no significant accumulation was detected in the parenchymal cells (Fig. 8, *panel A*). In the heart, the intense hybridization signal was detected in cardiac muscle cells (Fig. 8, *panel C*). The intense hybridization signals were also detected in bronchial epithelium and in alveolar macrophages in the lung (Fig. 8, *panel E*).

In contrast to the abundant expression of SRBI in steroidogenic tissues (3, 21), GPI-HBP1 transcripts were highly accumulated in the Kupffer cells as well as in alveolar macrophages of the lung. Based on the abundant expression in these scavenger cells and the lack of cholesterol efflux, it is suggested that GPI-HBP1 plays a role in the initial entry of HDL cholesterol into these scavenger cells for further transportation of cholesterol. To elucidate the precise biological role of GPI-HBP1 and to determine any disorders caused by the absence of the protein, the generation of mice lacking GPI-HBP1 is currently underway.

Acknowledgment—We thank Dr. M. Krieger for providing CHO ldlA7 cells.

REFERENCES

1. Krieger, M. (2001) *J. Clin. Invest.* **108,** 793–797
2. Acton, S. L., Scherer, P. E., Lodish, H. F., and Krieger, M. (1994) *J. Biol. Chem.* **269,** 21003–21009
3. Acton, S., Rigotti, A., Landschulz, K. T., Xu, S., Hobbs, H. H., and Krieger, M. (1996) *Science* **271,** 518–520
4. Tozuka, M., and Fidge, N. (1989) *Biochem. J.* **261,** 239–244
5. Matsumoto, A., Mitchell, A., Kurata, H., Pyle, L., Kondo, K., Itakura, H., and Fidge, N. (1997) *J. Biol. Chem.* **272,** 16778–16782
6. Matsuyama, A., Yamashita, S., Sakai, N., Maruyama, T., Okuda, E., Hirano, K., Kihara, S., Hiraoka, H., and Matsuzawa, Y. (2000) *Biochem. Biophys. Res. Commun.* **272,** 864–871
7. Nazih-Sanderson, F., Lestavel, S., Nion, S., Rouy, D., Denefle, P., Fruchart, J. C., Clavey, V., and Delbart, C. (1997) *Biochim. Biophys. Acta* **1358,** 103–112
8. Bocharov, A. V., Vishnyakova, T. G., Baranova, I. N., Patterson, A. P., and Eggerman, T. L. (2001) *Biochemistry* **40,** 4407–4416
9. Kozarsky, K. F., Donahee, M. H., Rigotti, A., Iqbal, S. N., Edelman, E. R., and Krieger, M. (1997) *Nature* **387,** 414–417
10. Rigotti, A., Trigatti, B. L., Penman, M., Rayburn, H., Herz, J., and Krieger, M. (1997) *Proc. Natl. Acad. Sci. U. S. A.* **94,** 12610–12615
11. Goldstein, J. L., Basu, S. K., and Brown, M. S. (1983) *Methods Enzymol.* **98,** 241–260
12. Kim, D. H., Iijima, H., Goto, K., Sakai, J., Ishii, H., Kim, H. J., Suzuki, H., Kondo, H., Saeki, S., and Yamamoto, T. (1996) *J. Biol. Chem.* **271,** 8373–8380
13. Takahashi, S., Kawarabayasi, Y., Nakai, T., Sakai, J., and Yamamoto, T. (1992) *Proc. Natl. Acad. Sci. U. S. A.* **89,** 9252–9256

14. Rigotti, A., Acton, S. L., and Krieger, M. (1995) *J. Biol. Chem.* **270,** 16221–16224
15. Sambrook, J., and Russell, D. W. (2001) in *Molecular Cloning: A Laboratory Manual*, 3rd Ed., Cold Spring Harbor Laboratory, Cold Spring Harbor, NY
16. Ishibashi, S., Brown, M. S., Goldstein, J. L., Gerard, R. D., Hammer, R. E., and Herz, J. (1993) *J. Clin. Invest.* **92,** 883–893
17. Kingsley, D. M., and Krieger, M. (1984) *Proc. Natl. Acad. Sci. U. S. A.* **81,** 5454–5458
18. Lowry, O. H., Rosebrough, N. J., Farr, A. L., and Randall, R. J. (1951) *J. Biol. Chem.* **193,** 265–275
19. Gu, X., Kozarsky, K., and Krieger, M. (2000) *J. Biol. Chem.* **275,** 29993–30001
20. Shan, X., Bourdeau, A., Rhoton, A., Wells, D. E., Cohen, E. H., Landgraf, B. E., and Palfree, R. G. (1998) *J. Immunol.* **160,** 197–208
21. Rigotti, A., Edelman, E. R., Seifert, P., Iqbal, S. N., DeMattos, R. B., Temel, R. E., Krieger, M., and Williams, D. L. (1996) *J. Biol. Chem.* **271,** 33545–33549

Low-density lipoprotein receptor-related protein 5 (LRP5) is essential for normal cholesterol metabolism and glucose-induced insulin secretion

Takahiro Fujino[a,b], Hiroshi Asaba[b,c], Man-Jong Kang[b,d], Yukio Ikeda[a,b,c], Hideyuki Sone[a,b], Shinji Takada[e,f,g], Dong-Ho Kim[a], Ryoichi X. Ioka[a], Masao Ono[h], Hiroko Tomoyori[i], Minoru Okubo[j], Toshio Murase[j], Akihisa Kamataki[a], Joji Yamamoto[a,c], Kenta Magoori[a], Sadao Takahashi[k], Yoshiharu Miyamoto[h], Hisashi Oishi[h], Masato Nose[h], Mitsuyo Okazaki[l], Shinichi Usui[l], Katsumi Imaizumi[i], Masashi Yanagisawa[c,m], Juro Sakai[a,c,n], and Tokuo T. Yamamoto[a]

[a]Gene Research Center and Division of Nephrology, Endocrinology, and Vascular Medicine, Department of Medicine, Tohoku University, Sendai 980-8574, Japan; [c]Yanagisawa Orphan Receptor Project, Exploratory Research for Advanced Technology, Japan Science and Technology Corporation, Tokyo 135-0064, Japan; [d]Department of Animal Science, College of Agriculture, Chonnam National University, Kwangju 500-600, Korea; [e]Graduate School of Science, Kyoto University, Kyoto 606-8502, Japan; [f]Kondoh Differentiation Signaling Project, Exploratory Research for Advanced Technology, Japan Science and Technology Corporation, Kyoto 606-8305, Japan; [g]Center for Integrative Bioscience, Okazaki, Aichi 444-8585, Japan; [h]Departments of Pathology and Orthopedics, Ehime University School of Medicine, Ehime 791-0295, Japan; [i]Laboratory of Nutritional Chemistry, Graduate School of Agriculture, Kyusyu University, Fukuoka 812-8581, Japan; [j]Department of Endocrinology and Metabolism, Toranomon Hospital, Tokyo 105-8470, Japan; [k]Third Department of Internal Medicine, Fukui Medical University, Fukui 910-1193, Japan; [l]Laboratory of Chemistry, College of Liberal Arts and Sciences, Tokyo Medical and Dental University, Chiba 282-0827, Japan; and [m]Howard Hughes Medical Institute, Department of Molecular Genetics, University of Texas Southwestern Medical Center, Dallas, TX 75235-9050

Edited by Michael S. Brown, University of Texas Southwestern Medical Center, Dallas, TX, and approved November 7, 2002 (received for review June 26, 2002)

A Wnt coreceptor low-density lipoprotein receptor-related protein 5 (LRP5) plays an essential role in bone accrual and eye development. Here, we show that LRP5 is also required for normal cholesterol and glucose metabolism. The production of mice lacking LRP5 revealed that LRP5 deficiency led to increased plasma cholesterol levels in mice fed a high-fat diet, because of the decreased hepatic clearance of chylomicron remnants. In addition, when fed a normal diet, LRP5-deficient mice showed a markedly impaired glucose tolerance. The LRP5-deficient islets had a marked reduction in the levels of intracellular ATP and Ca^{2+} in response to glucose, and thereby glucose-induced insulin secretion was decreased. The intracellular inositol 1,4,5-trisphosphate (IP3) production in response to glucose was also reduced in LRP5−/− islets. Real-time PCR analysis revealed a marked reduction of various transcripts for genes involved in glucose sensing in LRP5−/− islets. Furthermore, exposure of LRP5+/+ islets to Wnt-3a and Wnt-5a stimulates glucose-induced insulin secretion and this stimulation was blocked by the addition of a soluble form of Wnt receptor, secreted Frizzled-related protein-1. In contrast, LRP5-deficient islets lacked the Wnt-3a-stimulated insulin secretion. These data suggest that Wnt/LRP5 signaling contributes to the glucose-induced insulin secretion in the islets.

diabetes | Wnt protein | chylomicron remnant | pancreatic β cells | *insulin-like growth factor 1*

Low-density lipoprotein (LDL) receptor-related protein (LRP)5 and LRP6 are coreceptors involved in the Wnt signaling pathway (1–6). The Wnt signaling pathway plays a pivotal role in embryonic development (7, 8) and oncogenesis (9) through various signaling molecules including Frizzled receptors (10), recently characterized LRP5 and LRP6 (1–6), and Dickkopf proteins (4, 6). In addition, the Wnt signaling is also involved in adipogenesis by negatively regulating adipogenic transcription factors (Tcfs) (11). Although Wnt signaling has been characterized in both developmental and oncogenic processes, little is known about its function in the normal adult.

Recent studies have revealed that loss of function mutations in the LRP5 gene cause the autosomal recessive disorder osteoporosis–pseudoglioma syndrome (12). LRP5 is expressed in osteoblasts and transduces Wnt signaling via the canonical pathway, thereby modulating bone accrual development (12, 13). A point mutation in a "propeller" motif in LRP5 causes a dominant-positive high bone density by impairing the action of a normal antagonist of the Wnt pathway, Dickkopf, thereby increasing Wnt signaling (14, 15). In addition, the human LRP5 gene is mapped within the region (IDDM4) linked to type 1 diabetes on chromosome 11q13 (16).

In previous studies, we and others showed that LRP5 is highly expressed in many tissues, including hepatocytes and pancreatic beta cells (17, 18). We also showed that LRP5 can bind apolipoprotein E (apoE) (18). This finding raises the possibility that LRP5 plays a role in the hepatic clearance of apoE-containing chylomicron remnants, a major plasma lipoprotein carrying diet-derived cholesterol.

To evaluate the *in vivo* roles of LRP5, we generated LRP5-deficient mice. In this paper, we describe a function of LRP5 in the metabolism of cholesterol and glucose. Our data indicate that LRP5 is a multifunctional receptor involved in multiple pathways, including bone development, cholesterol metabolism, and the modulation of glucose-induced insulin secretion.

Experimental Procedures

Generation of LRP5-Deficient Mice. To produce mice carrying a mutated LRP5 gene, a targeting vector was constructed from a genomic DNA fragment containing exons 17 and 18 of the murine LRP5 gene. A neomycin-resistance gene under transcriptional control of the mouse phosphoglycerate kinase-1 promoter (PGK-neo) was inserted into the *Xho*I site within exon 18 of the mouse LRP5 gene. The 5′ and 3′ DNA fragments flanking PGK-neo were ligated into a pMCDT-A plasmid (GIBCO/BRL) composed of a poly(A)-less *neo* gene, a polymerase destabilizing signal, a pausing signal for RNA polymerase II, and the diphtheria toxin A fragment (DT-A) gene for negative selection (19). TT2 embryonic stem (ES) cells (20) were

This paper was submitted directly (Track II) to the PNAS office.

Abbreviations: apoE, apolipoprotein E; $[Ca^{2+}]_i$, intracellular Ca^{2+} concentration; CM, conditioned medium; HNF, hepatocyte nuclear factor; IGF, insulin-like growth factor; IRS, insulin receptor substrate; IP3, inositol 1,4,5-trisphosphate; LDL, low-density lipoprotein; LRP, LDL receptor-related protein; sFRP-1, secreted Frizzled-related protein-1; Tcf, transcription factor.

[b]T.F., H.A., M.-J.K., Y.I., and H.S. contributed equally to this work.

[n]To whom correspondence should be addressed at: Yanagisawa Orphan Receptor Project, Exploratory Research for Advanced Technology (ERATO), Japan Science and Technology Corporation (JST), National Museum of Emerging Science and Innovation, 2-41, Aomi, Koto-ku, Tokyo 135-0064, Japan. E-mail: jmsakai@mail.cc.tohoku.ac.jp or jmsakai@orphan.miraikan.jst.go.jp.

MEDICAL SCIENCES

transfected using standard techniques (21). Chimeric males were generated using the morula aggregation technique, and mated to C57BL/6J female mice. After achieving germ-line transmission, LRP5+/− females were crossed with C57BL/6J males. For immunoblotting, an antibody against murine LRP5 peptide (ATLYPPILNPPPSPA, amino acids 1490–1504, NCBI Protein database accession no. NP_032539) was generated. The antibody binding was detected with a chemiluminescence detection kit (ECL, no. RPN2106, Amersham Pharmacia Biotech).

Plasma Clearance and Hepatic Uptake of Chylomicron Remnants. Chylomicron remnants were prepared using a modified method of Redgrave and Martin (22) using functionally hepatectomized rats, and labeled with fluorescent lipid (1,1′-dioctadecyl-3,3,3′,3′-tetramethylindocarbocyanine perchlorate, DiI) as described by Takahashi *et al.* (23). Mice fed a high-fat diet for 16 weeks were injected i.v. into a femoral vein, with fluorescent chylomicron remnants from rat (5 μg per mouse) in 0.2 ml of PBS. Blood was sampled at various times and, after extracting lipid, plasma fluorescence was measured with a spectrofluorometer. The amount of fluorescence remaining in the plasma is expressed as a percentage of the calculated initial blood concentration, assuming that plasma volume is 4.4% (vol/wt) of body weight. After collection of the final blood samples, the mice were exsanguinated and livers were excised for the extraction of lipids and measurement of fluorescence.

Blood Glucose and Serum Insulin. Mice (6–8 months old) were fasted for 12 h and then given an i.p. injection of glucose (1 g/kg of body weight). Blood samples were obtained from the tail vein at the indicated times after the glucose load. Blood glucose and plasma insulin levels were measured with the Glucose CII test Wako (Wako Pure Chemical, Osaka) and an insulin RIA kit (Shionogi, Osaka), respectively.

Analysis of Pancreatic Islets. The procedure for the isolation of pancreatic islets is described in *Supporting Methods*, which is published as supporting information on the PNAS web site, www.pnas.org. For the measurement of insulin secretion from islets, pancreatic islets from 6- to 8-month-old mice were pooled and cultured in RPMI medium 1640 containing 11.6 mM glucose, 1% penicillin–streptomycin, 10% FBS, and 25 mM Hepes at pH 7.4 (medium A). Pancreatic islets cells were infected with recombinant adenoviruses encoding LRP5 (AdLRP5) (18) or LacZ (AdLacZ) according to the procedure by Becker *et al.* (24). After culturing for 16–20 h, islets were transferred to Krebs–Ringer buffer (KRB; Sigma) containing 0.2% BSA for the measurement of insulin secretion studies by using an RIA kit (Amersham Pharmacia Biotech). For measurement of intracellular Ca^{2+} concentration ($[Ca^{2+}]_i$), pancreatic islet cells were cultured on a collagen-coated, glass-bottomed well for 16 h in medium A, and loaded with the fluorescent Ca^{2+} indicator Fluo3/AM as described by Katoh *et al.* (25). Changes in $[Ca^{2+}]_i$ were measured using a confocal laser scanning microscope (Axiovert 100, Zeiss) with a ×40 objective lens. Intracellular levels of ATP and ADP were measured with a luciferase–luciferin system by using an ATP determination kit (catalog number A-22066, Molecular Probes; ref. 26). Intracellular levels of inositol 1,4,5-trisphosphate (IP3) were determined using an IP3 RIA kit (Amersham Pharmacia Biotech).

Wnt-Conditioned Media (CM) and Purified Secreted Frizzled-Related Protein-1 (sFRP-1). CM from Wnt-3a, Wnt-5a, and parental vector-transfected L cells were prepared according to Shibamoto *et al.* (27). CM were diluted 5-fold with medium A. After incubation with CM for 16 h, islets were transferred to Krebs–Ringer buffer for the measurement of insulin for secretion studies.

An expression plasmid encoding recombinant sFRP-1 containing Myc/polyhistidine epitopes (28) was used to produce recombinant sFRP-1 in COS7 cells. COS7 cells were transfected with the expression plasmid by using the Lipofectamine reagent (GIBCO/BRL). Twenty-four hours after the transfection, the cells were switched to a serum-free medium (OPTI-PRO, GIBCO/BRL) and cultured for 48 h. Recombinant sFRP-1 was purified from the culture medium of transfected cells by using a HisTrap kit (Amersham Pharmacia Biotech) according to the manufacturer's protocol. The purity of the purified protein was verified by immunoblot analysis with anti-Myc tag antibody (Cell Signaling Technology, Beverly, MA).

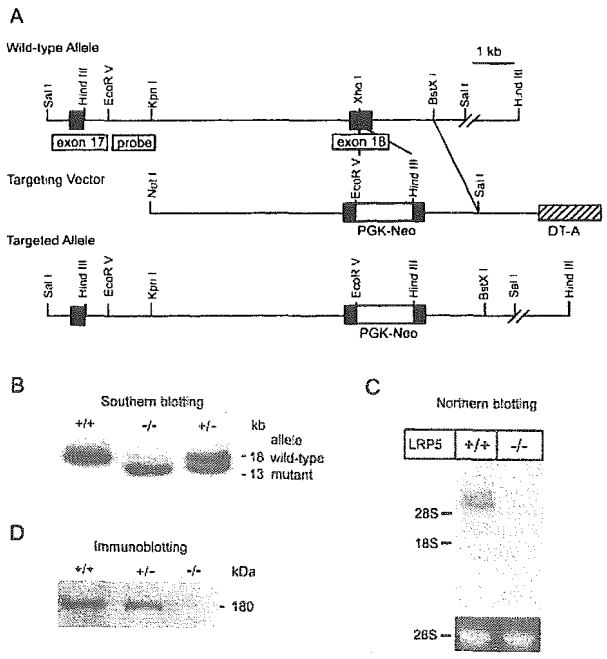

Fig. 1. Generation of LRP5-deficient mice. (*A*) Diagram of the targeting strategy. Only the relevant restriction sites are indicated. (*B*) Southern blot analysis of *Hin*dIII-digested DNA from LRP5+/+, LRP5−/−, and LRP5+/− mice. Southern blotting was performed with the probe indicated in *A*. *Hin*dIII digestion resulted in an 18-kb fragment in wild-type DNA and a 13-kb fragment in homologous recombinants. A typical autoradiogram is shown. (*C*) Northern blot analysis of LRP5 transcripts. Total RNA (15 μg) from the livers of LRP5+/+ and LRP5−/− mice was hybridized with a mouse LRP5 cDNA probe (extended from nucleotide 2401 to nucleotide 2991). A typical autoradiogram (48-h exposure) is shown. RNA loading was consistent among the lanes as judged by ethidium bromide staining and reprobing with glyceraldehyde-3-phosphate dehydrogenase. (*D*) Immunoblot analysis, using an anti-mouse LRP5 antibody, of LRP5+/+, LRP5+/−, and LRP5−/− mouse liver membrane fractions. Each lane was loaded with 500 μg of crude membrane fraction from the liver homogenates. Protein loading was consistent among the lanes as judged by Ponceau staining.

Results

Generation of LRP5-Deficient Mice. An insertion-type vector was constructed to disrupt an exon encoding a ligand-binding repeat of the mouse LRP5 gene (exon 18; Fig. 1*A*). Three lines of mice lacking LRP5 were identified by Southern blotting (Fig. 1*B*), and the absence of LRP5 transcripts (Fig. 1*C*) and protein (Fig. 1*D*) in the liver was confirmed by Northern blot and immunoblot analyses, respectively.

Wild-type (LRP5+/+), heterozygous (LRP5+/−), and homozygous (LRP5−/−) mice were born with frequencies predicted by simple Mendelian ratios. In contrast to the severe developmental defects of LRP6 mutant mice (3), LRP5−/− mice of both sexes developed and appeared normal, gaining weight at a rate equal to that of LRP5+/+ mice and were normally fertile. Under light-

microscopic examination of LRP5-deficient males, there were no apparent histological abnormalities in the tissues examined, including bone, brain, eye, kidney, liver, and pancreas.

Although no apparent low-bone-mass phenotype was observed in 3- to 6-month-old LRP5−/− males under light-microscopic examination, we noticed that the femur and parietal bones were thin and fragile in LRP5−/− females older than 6 months. The thickness of the parietal portion of calvaria of LRP5−/− mice was significantly reduced to 50–60% of the controls ($n = 3$, $P < 0.04$; Fig. 6, which is published as supporting information on the PNAS web site). Similarly, the thickness of tibias of LRP5−/− females was also reduced to 60–70% of the controls (data not shown). We also found some cases of pathological fracture of lower limbs in these mice. Recently, Kato *et al.* (13) generated LRP5−/− mice developing a severe low-bone-mass phenotype similar to that of patients with osteoporosis-pseudoglioma syndrome. The low-bone-mass phenotype of LRP5−/− generated by Kato *et al.* was observed regardless of sex and age, and a significant number of the mice died within the first month of life because of fractures. The relatively modest bone phenotype of our LRP5−/− females resembles the osteoporosis of humans and suggests that the involvement of other factors, including sex, aging, hormonal status, dietary exposure, and genetic background in the development of a low-bone-mass phenotype.

Impaired Chylomicron Clearance. To determine the metabolic consequences of LRP5 deficiency, we analyzed the effects of LRP5 deficiency on lipoprotein metabolism by using LRP5−/−, +/−, and +/+ mice. The plasma levels of cholesterol in LRP5+/− and LRP5−/− mice that were fed a standard laboratory chow were identical to those of their LRP5+/+ littermates (Fig. 7, which is published as supporting information on the PNAS web site). In contrast, when mice were fed a high-fat diet containing 7.5% coconut oil and 1.25% cholesterol, plasma cholesterol levels were significantly increased in both LRP5+/− and LRP5−/− mice. The levels of plasma cholesterol in LRP5−/− mice fed a high-fat diet for 2 months were ≈200 mg/dl, whereas those in LRP5+/+ littermates were ≈170 mg/dl (Fig. 2*A*). HPLC analysis of the plasma lipoprotein profile revealed that very low-density lipoprotein cholesterol was increased in LRP5−/− mice after being fed a high-fat diet (Fig. 7). The levels of plasma triglyceride in LRP5+/+ and −/− mice were indistinguishable (within the range of 50–80 mg/dl).

apoE-containing chylomicron remnants can be cleared normally in LDL receptor-lacking familial hypercholesterolemia patients and Watanabe hereditary hyperlipidemic rabbits (29). To determine the effects of LRP5 deficiency on the plasma clearance of chylomicron remnants, we injected fluorescently labeled chylomicron remnants into LRP5−/− mice and +/+ littermates fed a high-fat diet. As shown in Fig. 2*B*, approximately half of the injected chylomicron remnants were cleared from the plasma of LRP5+/+ mice at 30 min after injection, whereas >80% remained in the plasma of LRP5−/− mice. Consistent with the delayed clearance, hepatic uptake of the injected fluorescence was markedly reduced in LRP5−/− mice (≈16% of LRP5+/+ mice, Fig. 2*C*). A similar result was obtained for apoE-rich β-migrating very low-density lipoprotein (data not shown). The mRNA levels of LDL receptor and LRP1 (a candidate chylomicron remnant receptor; ref. 30), were indistinguishable between LRP5+/+ and −/− mice (data not shown). These data indicate that LRP5 recognizes apoE-containing lipoproteins *in vivo* and plays a role in the hepatic clearance of chylomicron remnants.

Impaired Glucose-Induced Insulin Secretion. We next analyzed the effects of LRP5 deficiency on glucose metabolism in LRP5−/− mice. Mice were fed either a normal laboratory chow diet (CE-2, CLEA Japan, Osaka) or a high-fat diet containing 1.5% cholesterol, 7.5% olive oil, 5% cholic acid, and 7.5% milk casein in a standard

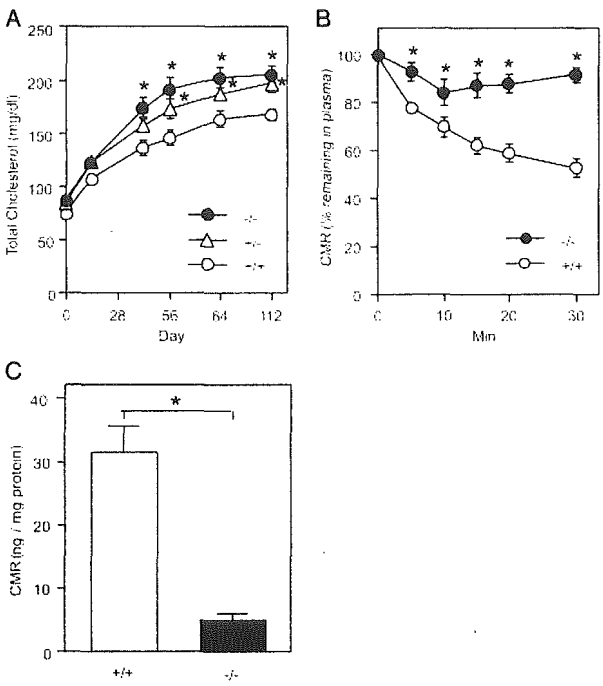

Fig. 2. Diet-induced hypercholesterolemia in LRP5-deficient mice. (*A*) Total plasma cholesterol levels in mice that were fed a high-fat diet. Mice (7–8 weeks of age) heterozygous (LRP5+/−) and homozygous (LRP5−/−) for LRP5 deficiency and their wild-type littermates (LRP5+/+) were fed a high-fat diet for 16 weeks, during which plasma total cholesterol levels of each mouse were measured at the indicated times. The values are the mean ± SE for six mice. *, $P < 0.05$ compared with LRP5+/+. (*B* and *C*) Plasma clearance (*B*) and liver uptake (*C*) of injected chylomicron remnants (CMR). The values are the mean ± SE for six mice. *, $P < 0.01$; Student's *t* test.

laboratory chow diet. Although fasted blood glucose and insulin levels in LRP5−/− and +/− mice appeared identical to those of their +/+ littermates, even after being fed a high-fat diet (90–110 mg/dl), LRP5−/− and LRP5+/− mice exhibited impaired glucose tolerance (IGT) during an i.p. glucose-tolerance test (Fig. 3*A*). This IGT was observed regardless of sex; however, it was age-dependent, because significant glucose intolerance was not seen in LRP5-deficient mice before 6 months of age. Consistent with the marked glucose intolerance, the glucose-induced increase in plasma insulin concentration was lower in both LRP5−/− and LRP5+/− mice than in LRP5+/+ mice (Fig. 3*B*). Pancreatic sections from 6-month-old LRP5+/+ and LRP5−/− mice showed no manifestation of insulitis, including the infiltration of lymphocytes or reduced cell mass in LRP5−/− islets (Fig. 8*A*, which is published as supporting information on the PNAS web site). Similarly, the appearances of alpha and beta cells of the islets were almost indistinguishable in LRP5+/+ and −/− mice as determined by Grimelius (alpha cells; Fig. 8*B*) and aldehyde–fuchsin staining (beta cells; Fig. 8*C*). Pancreatic insulin levels in LRP5−/− mice were not significantly different from those of LRP5+/+ mice and are as follows: 7.07 ± 0.94 and 6.40 ± 0.48 milliunits/mg of protein in LRP5+/+ and LRP5−/− mice, respectively ($n = 6$; Fig. 8*D*). Pancreas weights were also indistinguishable in LRP5+/+ and −/− mice (306 ± 17 and 296 ± 8 mg in LRP5+/+ and LRP5−/− mice, respectively, $n = 6$). No apparent differences were seen in the size of the islets between LRP5+/+ and −/− mice either, as shown in Table 3, which is published as supporting information on the PNAS web site. An i.p. insulin tolerance test revealed that LRP5−/− mice fed a normal diet were not insulin resistant (data not shown). In contrast to LRP5−/− mice, IGT was not seen in mice lacking apoE (data not shown), suggesting that the IGT in

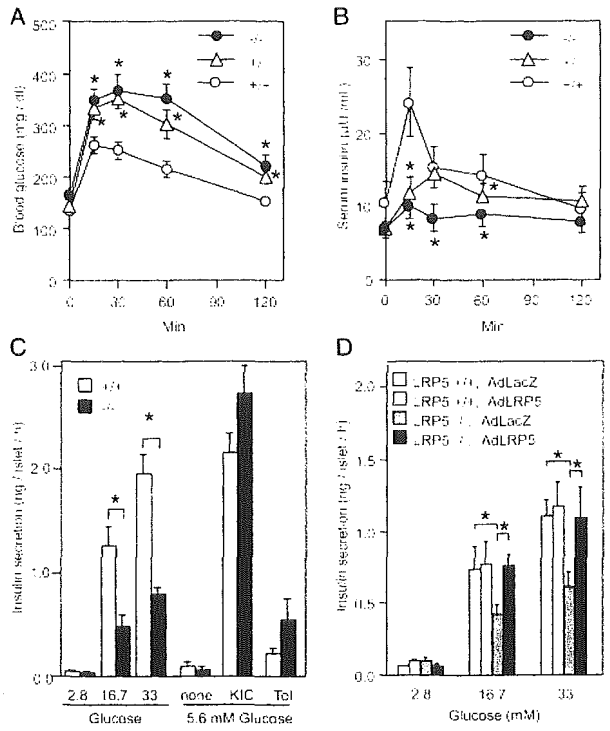

Fig. 3. Impaired glucose-induced insulin secretion in LRP-deficient mice and amelioration by AdLRP5. (*A* and *B*) Blood glucose (*A*) and serum insulin (*B*) levels in LRP5+/+, +/−, and −/− mice after glucose injection. (*C*) Impaired insulin secretion from the islets of LRP5−/− mice. Insulin secretion was induced by different concentrations of glucose and 0.2 mM tolbutamide (Tol), or 10 mM α-ketoisocaproate (KIC), in the presence of 5.6 mM glucose. (*D*) Restoration of insulin secretion by AdLRP5. Pancreatic islets were isolated from LRP5+/+ and −/− mice, infected with recombinant adenoviruses encoding LRP5 (AdLRP5) or LacZ (AdLacZ), and insulin secretion was measured at various glucose concentrations. The values in *A* and *B* are the mean ± SE for six mice; those in *C* and *D* are the mean ± SE for four mice. *, $P < 0.01$; Student's *t* test.

LRP5+/− and −/− mice is independent of apoE binding to LRP5. Although LRP5−/− islets showed impaired glucose-induced insulin secretion, no apparent insulin resistance was observed in LRP5−/− mice. Other factors, including aging, obesity, and prolonged high-fat feeding, may therefore be required to induce typical type 2 diabetes in LRP5−/− mice.

To further define the effects of LRP5 deficiency on glucose-induced insulin secretion, pancreatic islets were prepared from LRP5+/+ and −/− mice, and the changes in the levels of glucose-induced insulin secretion were analyzed. Consistent with the glucose-tolerance test, the change in the insulin secretory response to glucose in LRP5−/− islets was profoundly lower than that of LRP5+/+ islets, particularly at higher concentrations (Fig. 3*C*). When islets were incubated with 10 mM α-ketoisocaproate, which is used for ATP production (31), the changes in the levels of insulin secretion from islets of LRP5−/− mice were approximately the same as those from LRP5+/+ mice, suggesting that there is no impaired ATP production from α-ketoisocaproate in the mitochondrial tricarboxylic acid cycle. Similarly, when cells were incubated with 0.2 mM tolbutamide, there were no changes in the levels of insulin secretion in LRP5−/− and +/+ mice. To restore the impaired insulin secretory response to glucose, LRP5−/− islets were infected with recombinant adenovirus encoding human LRP5 (AdLRP5). As shown in Fig. 3*D*, infection of LRP5−/− islets with AdLRP5 caused their glucose-induced insulin secretion to recover to the levels of LRP5+/+ islets infected with control adenovirus encoding β-galactosidase (AdLacZ) or AdLRP5.

To further evaluate the impaired glucose-induced insulin secretion in LRP5−/− islets, we compared ATP and ADP levels in the islets. As shown in Table 1, the ATP content and ATP/ADP ratio in the presence of 22.2 mM glucose were significantly decreased (by 25–30%) in LRP5−/− islets compared with those in +/+ islets. In contrast, the glycogen content of the islets and hepatic glycogen synthase activity were almost unaltered in LRP5−/− mice (data not shown). Taken together, these data (Fig. 3*C* and Table 1) suggest that the glycolytic pathway was impaired in the LRP5−/− islets.

Consistent with the decreased ATP content and ATP/ADP ratio, glucose-induced intracellular $[Ca^{2+}]_i$ level was markedly decreased in uninfected LRP5-deficient islets. Fig. 4*A* and *B* shows the glucose-induced $[Ca^{2+}]_i$ increase (as determined by changes in fluorescence intensity) in LRP5+/+ and −/−islets infected with AdLacZ or AdLPR5. The glucose-induced $[Ca^{2+}]_i$ increase in LRP5−/− islets infected with AdLacZ (Fig. 4*B*) was markedly lower than that of LRP5+/+ islets infected with AdLacZ or AdLRP5 (Fig. 4*A*). The average changes in fluorescence intensity (in arbitrary units) by glucose (2.8 mM → 20 mM) in LRP5−/− and LRP5+/+ islets infected with AdLacZ were 29.85 ± 4.04 and 11.10 ± 1.36, respectively ($n = 30$; $P < 0.001$). When LRP5-deficient islets were infected with AdLRP5, the glucose-induced $[Ca^{2+}]_i$ was restored almost completely to normal levels (Fig. 4*B*). There were no statistical differences in the increases in $[Ca^{2+}]_i$ among LRP5+/+ islets infected with AdLacZ or AdLRP5 and LRP5−/−islets infected with AdLRP5. We also examined the glucose-induced production of IP3. The glucose-induced intracellular levels of IP3 were profoundly reduced in LRP5−/− islets (Fig. 4*C*). When LRP5-deficient islets were infected with AdLRP5, the glucose-induced IP3 production was restored almost completely to normal levels (Fig. 4*D*).

Real-Time PCR Analysis. To identify the mechanism underlying the impaired glucose-stimulated insulin secretion, especially the reduced glycolytic pathway, we evaluated steady-state mRNA levels of glucose-sensing proteins and the hepatocyte nuclear factor (HNF) family of transcriptional factors by real-time PCR (see *Supporting Methods*). As shown in Table 2, the mRNA levels of insulin-like growth factor (IGF)-1 receptor, insulin receptor

Table 1. ATP and ADP contents and the ATP/ADP ratio in glucose-stimulated islets

	LRP5+/+		LRP5−/−	
Measurement	2.8 mM glucose	22.2 mM glucose	2.8 mM glucose	22.2 mM glucose
ATP, pmol/islet	4.69 ± 0.08	9.95 ± 0.78	5.20 ± 0.16	7.91 ± 0.74*
ADP, pmol/islet	2.66 ± 0.23	1.89 ± 0.07	1.93 ± 0.15	1.81 ± 0.10
ATP/ADP ratio	2.10 ± 0.23	4.93 ± 0.07	2.31 ± 0.12	3.37 ± 0.20**

Islets of four mice were pooled and incubated at 37°C in the presence of 2.8 or 22.2 mM glucose. After 1 h, the incubation was stopped by the addition of 0.125 ml of trichloroacetic acid to a final concentration of 5%. The islets were disrupted by sonication, and ATP and ADP contents were measured with a luciferase–luciferin system (25). Data are from four independent experiments. Each value represents the mean ± SE. *, $P < 0.01$; **, $P < 0.001$; as compared with wild-type islets (one-way ANOVA).

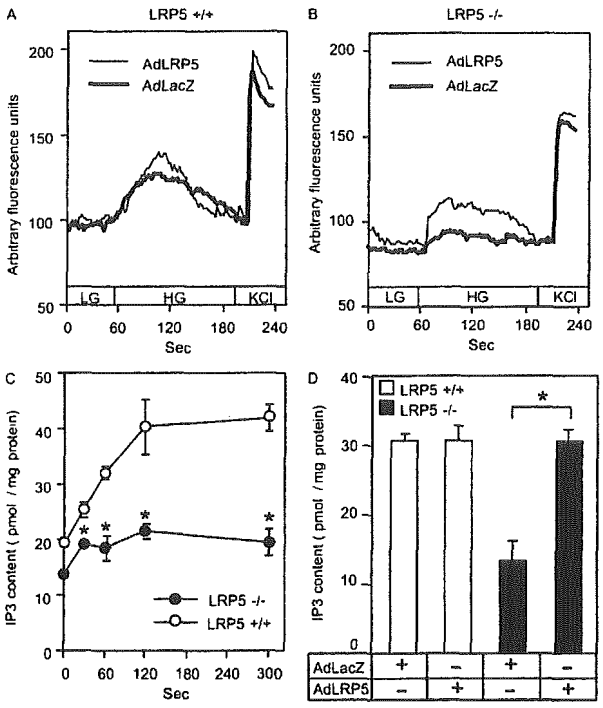

Fig. 4. *Impaired glucose-induced $[Ca^{2+}]_i$ increase and IP3 production in* LRP5-deficient islets. (*A* and *B*) LRP5+/+ (*A*) and −/− (*B*) islets infected with AdLRP5 or control AdLacZ. Changes in $[Ca^{2+}]_i$ were measured under low glucose (2.8 mM; LG), high glucose (20 mM; HG), or 20 mM KCl (KCl). Representative data from 30 experiments are shown. (*C*) Time course of IP3 content in response to 20 mM glucose in LRP5+/+ and −/− islets. Values are the mean ± SE from quadruplicate determinations. (*D*) Restoration of IP3 production by AdLRP5. Pancreatic islet cells were isolated from LRP5+/+ and −/− mice and infected with AdLRP5 or AdLacZ, and the IP3 content was measured at 5 min after exposure to 20 mM glucose. The values are the mean ± SE from quadruplicate determinations. *, $P < 0.01$; Student's *t* test.

substrate-2 (IRS-2), HNF-4α, insulin receptor, and Tcf1 (HNF-1α) transcripts were drastically decreased in LRP5−/− islets (3%, 6%, 9%, 12%, and 17% of control, respectively). Similarly, the levels of Tcf2 (HNF-1β), glucokinase, Foxa1 (Forkhead box A1, HNF-3α), and Tcf4 transcripts were profoundly decreased in LRP5−/− islets (33%, 49%, 51%, and 59% of control, respectively). In contrast, the levels of glucose transporter 2 were unchanged and the insulin transcripts were increased by 30% in LRP5−/− islets.

Effects of Wnt on Glucose-Induced Insulin Secretion. LRP5 has been shown to bind Wnt and believed to act as a coreceptor for the Wnt signaling pathway. To determine the involvement of Wnt proteins in glucose-induced insulin secretion, we pretreated LRP5+/+ islets with CM from Wnt-3a-, Wnt-5a-, or parental vector-transfected L cells (neo-CM) (27). As shown in Fig. 5*A*, pretreatment of LRP5+/+ islets with Wnt-3a-, and Wnt-5a CM for 16 h markedly stimulated glucose-induced insulin secretion. This Wnt protein-stimulated glucose-induced insulin secretion was blocked by the addition of purified Frizzled-related protein-1 (*FRP1* gene product), a soluble antagonist for sFRP-1 (28).

In contrast, this stimulation of glucose-induced insulin secretion by Wnt-3a-CM was not seen in uninfected LRP5-deficient islets (data not shown) or in LRP5−/− islets infected with AdLacZ, whereas AdLRP5 infection restored the Wnt-3a-stimulated insulin secretion (Fig. 5*B*). These data demonstrate that Wnt-3a-stimulated glucose-induced insulin secretion is mediated by LRP5. In contrast to the stimulation by Wnt-3a of glucose-induced insulin secretion, the intracellular insulin levels

Table 2. Relative amounts of mRNAs in islets from LRP5−/− mice as compared with values in +/+ mice

mRNA from islets	Relative amount of mRNA in LRP5−/− mice
Tcf1 (HNF-1α)	0.17
Tcf2 (HNF-1β)	0.33
Tcf4	0.59
Foxa1 (HNF-3α)	0.51
Foxa2 (HNF-3β)	0.85
HNF-4α	0.09
Insulin	1.30
IRS-1	0.60
IRS-2	0.06
Insulin receptor	0.12
IGF-1	1.78
IGF-2	0.64
IGF-1 receptor	0.03
Glucose transporter 2	0.94
Glucokinase	0.49
LRP5	0.01

Male mice aged 6–8 months were used in this experiment. Total RNA from islets of four mice was pooled and subjected to real-time PCR quantification as described under *Experimental Procedures*. Cyclophilin was used as the invariant control. Values represent the amount of mRNA relative to that in LRP5+/+ mice, which is arbitrarily defined as 1.

were unchanged, indicating that Wnt-3a has no effects on the production of insulin in the islets (data not shown).

Discussion

Here, we investigated the function of LRP5 by examining LRP5−/− mice. We show that LRP5 is required for proper hepatic clearance of chylomicron remnants and for glucose-induced insulin secretion from the pancreatic islets, in addition to bone and eye development. Hyperlipoproteinemia has long been known to be a significant complication of diabetes, and our studies suggest a possible molecular linkage through LRP5. So far, the LRP5 locus has been linked to type 1 diabetes (32, 33) in humans, and our studies indicate that a more detailed investigation of the linkage of LRP5 with type 2 diabetes is warranted.

Consistent with the impaired glucose-induced insulin secretion and the reduced ATP/ADP ratio in LRP5−/− islets, the

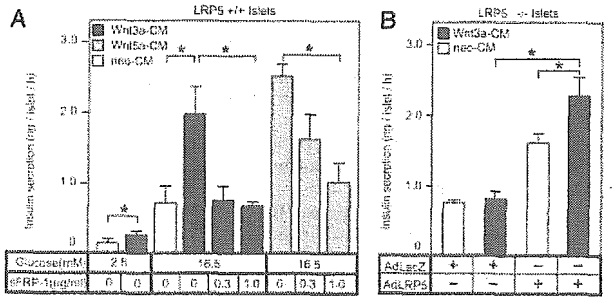

Fig. 5. Effects of Wnt-3a and Wnt-5a on glucose-induced insulin secretion. (*A*) Insulin secretion from the islets. LRP5+/+ islets were pretreated with 5-fold diluted Wnt-3a-CM, Wnt-5a-CM, or control neo-CM in the presence of the indicated concentration of sFRP-1 for 16 h before measuring insulin secretion induced by glucose. (*B*) Lack of Wnt-3a stimulation of insulin secretion from LRP5-deficient islets and restoration by AdLRP5. LRP5−/− islets were infected with AdLRP5 or AdLacZ and exposed to Wnt-3a- or control neo-CM for 16 h before measuring insulin secretion in the presence of 16.5 mM glucose. The values are the mean ± SE for four mice from quadruplicate determinations. *, $P < 0.01$; Student's *t* test.

steady-state levels of mRNAs for several important molecules in the islets were profoundly decreased. These include the HNF family of transcriptional factors (Tcf1, Tcf2, Foxa1, and HNF-4α,), glucose-sensing protein (glucokinase), and insulin-signaling proteins (insulin receptor, IGF-1 receptor, and IRS-2). Mutations in Tcf1, Tcf2, and HNF-4α genes impair insulin secretion and cause mature-onset diabetes of the young (MODY). Insulin signaling through the insulin receptor is important for maintaining the transcriptional level of glucokinase and insulin itself in beta cells (34–36). Also, the IGF-1 receptor signaling pathway through IRS-2 mediates the beta cell compensation for peripheral insulin resistance, as well as the development, proliferation, and survival of beta cells (37, 38). Our data provide the evidence that LRP5 together with Wnt maintains the normal function of the β cells through the transcriptional regulation of the above-mentioned genes.

Glycogen synthase kinase β (GSK3β) is a key component in many biological processes, including insulin- and Wnt-signaling pathways. Both insulin and Wnt inactivate GSK3β although through different mechanisms: phosphorylation mediated by Akt/PKB and axin conduction complex, respectively. Whereas insulin induces glycogen synthase activity through the inactivation of GSK3β, Wnt had no effect on glycogen synthase activity (39). Despite the marked reduction of steady-state insulin receptor transcripts in LRP5$-/-$ islets, the glycogen content of the islets, hepatic glycogen synthase activity, and pancreatic insulin content were almost unchanged in LRP5$-/-$ mice. In the beta cell-specific knockout for the insulin receptor, there is a decrease in glucose-stimulated insulin release and a marked reduction the insulin content of the cells (35). In contrast, the insulin content in the islets is unaltered in the beta cell-specific knockout for IGF receptor, whereas glucose-stimulated insulin secretion is markedly impaired (38). Based on the similarity of glucose-sensing defects between the mice lacking LRP5 and beta cell-specific IGF receptor, and the drastic reduction of IGF receptor transcripts in LRP5$-/-$ islets, it is suggested that IGF signaling is impaired in LRP5$-/-$ islets.

Despite the differences in the biological roles of Wnt-3a and Wnt-5a (β-catenin/Wnt pathway and Ca^{2+}/Wnt pathway, respectively), both proteins have similar effects on the stimulation of glucose-induced insulin secretion. Based on the stimulation of glucose-induced insulin secretion by Wnt proteins and the lack of the Wnt-stimulated insulin secretion in LRP5 deficient islets, we conclude that LRP5 together with Wnt proteins modulates glucose-induced insulin secretion. Although the precise pathway for Wnt signaling in the islets is currently unknown, this work has demonstrated that Wnt proteins are involved in normal glucose metabolism in the adult mouse and suggests that the Wnt pathway may provide novel therapeutic strategies for the treatment of type 2 diabetes.

We thank Drs. M. S. Brown and J. L. Goldstein for helpful discussion and critical reading of this manuscript; T. F. Osborne, P. Espenshade, H. Okamoto, H. Takeshima, and S. Takasawa for helpful advice; I. Gleadall for review of the manuscript; J. Rubin for sFRP-1 plasmid; A. Yamashita and T. Kadowaki for valuable advice on ATP and ADP measurement; S. Iwasaki for excellent technical advice on the glycogen measurement; H. Iguchi for technical help with real-time PCR; K. Katoh for assistance with Ca^{2+} measurement; and Y. Takei, M. Sasaki, S. Takahashi, and R. Nagata for excellent technical assistance. This work was supported in part by Japan Society for Promotion of Science Grant RFTF97L00803 and Japan Science and Technology Corporation/Exploratory Research for Advanced Technology (Yanagisawa Orphan Receptor Project).

1. Wehrli, M., Dougan, S. T., Caldwell, K., O'Keefe, L., Schwartz, S., Vaizel-Ohayon, D., Schejter, E., Tomlinson, A. & DiNardo, S. (2000) *Nature* **407,** 527–530.
2. Tamai, K., Semenov, M., Kato, Y., Spokony, R., Liu, C., Katsuyama, Y., Hess, F., Saint-Jeannet, J. P. & He, X. (2000) *Nature* **407,** 530–535.
3. Pinson, K. I., Brennan, J., Monkley, S., Avery, B. J. & Skarnes, W. C. (2000) *Nature* **407,** 535–538.
4. Bafico, A., Liu, G., Yaniv, A., Gazit, A. & Aaronson, S. A. (2001) *Nat. Cell Biol.* **3,** 683–686.
5. Mao, J., Wang, J., Liu, B., Pan, W., Farr, G. H., III, Flynn, C., Yuan, H., Takada, S., Kimelman, D., Li, L. & Wu, D. (2001) *Mol. Cell* **7,** 801–809.
6. Mao, B., Wu, W., Li, Y., Hoppe, D., Stannek, P., Glinka, A. & Niehrs, C. (2001) *Nature* **411,** 321–325.
7. Nusse, R. & Varmus, H. E. (1992) *Cell* **69,** 1073–1087.
8. Wodarz, A. & Nusse, R. (1998) *Annu. Rev. Cell Dev. Biol.* **14,** 59–88.
9. Sparks, A. B., Morin, P. J., Vogelstein, B. & Kinzler, K. W. (1998) *Cancer Res.* **58,** 1130–1134.
10. Bhanot, P., Brink, M., Samos, C. H., Hsieh, J. C., Wang, Y., Macke, J. P., Andrew, D., Nathans, J. & Nusse, R. (1996) *Nature* **382,** 225–230.
11. Ross, S. E., Hemati, N., Longo, K. A., Bennett, C. N., Lucas, P. C., Erickson, R. L. & MacDougald, O. A. (2000) *Science* **289,** 950–953.
12. Gong, Y., Slee, R. B., Fukai, N., Rawadi, G., Roman-Roman, S., Reginato, A. M., Wang, H., Cundy, T., Glorieux, F. H., Lev, D., *et al.* (2001) *Cell* **107,** 513–523.
13. Kato, M., Patel, M. S., Levasseur, R., Lobov, I., Chang, B. H., Glass, D. A., Jr., Hartmann, C., Li, L., Hwang, T. H., Brayton, C. F., *et al.* (2002) *J. Cell Biol.* **157,** 303–314.
14. Little, R. D., Carulli, J. P., Del Mastro, R. G., Dupuis, J., Osborne, M., Folz, C., Manning, S. P., Swain, P. M., Zhao, S. C., Eustace, B., *et al.* (2002) *Am. J. Hum. Genet.* **70,** 11–19.
15. Boyden, L. M., Mao, J., Belsky, J., Mitzner, L., Farhi, A., Mitnick, M. A., Wu, D., Insogna, K. & Lifton, R. P. (2002) *N. Engl. J. Med.* **346,** 1513–1521.
16. Hey, P. J., Twells, R. C., Phillips, M. S., Yusuke, N., Brown, S. D., Kawaguchi, Y., Cox, R., Guochun, X., Dugan, V., Hammond, H., *et al.* (1998) *Gene* **216,** 103–111.
17. Figueroa, D. J., Hess, J. F., Ky, B., Brown, S. D., Sandig, V., Hermanowski-Vosatka, A., Twells, R. C., Todd, J. A. & Austin, C. P. (2000) *J. Histochem. Cytochem.* **48,** 1357–1368.
18. Kim, D. H., Inagaki, Y., Suzuki, T., Ioka, R. X., Yoshioka, S. Z., Magoori, K., Kang, M. J., Cho, Y., Nakano, A. Z., Liu, Q., *et al.* (1998) *J. Biochem. (Tokyo)* **124,** 1072–1076.
19. Yagi, T., Nada, S., Watanabe, N., Tamemoto, H., Kohmura, N., Ikawa, Y. & Aizawa, S. (1993) *Anal. Biochem.* **214,** 77–86.
20. Yagi, T., Tokunaga, T., Furuta, Y., Nada, S., Yoshida, M., Tsukada, T., Saga, Y., Takeda, N., Ikawa, Y. & Aizawa, S. (1993) *Anal. Biochem.* **214,** 70–76.
21. Abrahamsohn, P. A. & Zorn, T. M. (1993) *J. Exp. Zool.* **266,** 603–628.
22. Redgrave, T. G. & Martin, G. (1977) *Atherosclerosis (Shannon, Irel.)* **28,** 69–80.
23. Takahashi, S., Kawarabayasi, Y., Nakai, T., Sakai, J. & Yamamoto, T. (1992) *Proc. Natl. Acad. Sci. USA* **89,** 9252–9256.
24. Becker, T. C., BeltrandelRio, H., Noel, R. J., Johnson, J. H. & Newgard, C. B. (1994) *J. Biol. Chem.* **269,** 21234–21238.
25. Katoh, K., Komatsu, T., Yonekura, S., Ishiwata, H., Hagino, A. & Obara, Y. (2001) *J. Endocrinol.* **169,** 381–388.
26. Detimary, P., Van den Berghe, G. & Henquin, J. C. (1996) *J. Biol. Chem.* **271,** 20559–20565.
27. Shibamoto, S., Higano, K., Takada, R., Ito, F., Takeichi, M. & Takada, S. (1998) *Genes Cells* **3,** 659–670.
28. Uren, A., Reichsman, F., Anest, V., Taylor, W. G., Muraiso, K., Bottaro, D. P., Cumberledge, S. & Rubin, J. S. (2000) *J. Biol. Chem.* **275,** 4374–4382.
29. Kita, T., Goldstein, J. L., Brown, M. S., Watanabe, Y., Hornick, C. A. & Havel, R. J. (1982) *Proc. Natl. Acad. Sci. USA* **79,** 3623–3627.
30. Rohlmann, A., Gotthardt, M., Hammer, R. E. & Herz, J. (1998) *J. Clin. Invest.* **101,** 689–695.
31. Ashcroft, S. J. (1997) *Adv. Exp. Med. Biol.* **426,** 73–80.
32. Nakagawa, Y., Kawaguchi, Y., Twells, R. C., Muxworthy, C., Hunter, K. M., Wilson, A., Merriman, M. E., Cox, R. D., Merriman, T., Cucca, F., *et al.* (1998) *Am. J. Hum. Genet.* **63,** 547–556.
33. Twells, R. C., Metzker, M. L., Brown, S. D., Cox, R., Garey, C., Hammond, H., Hey, P. J., Levy, E., Nakagawa, Y., Philips, M. S., *et al.* (2001) *Genomics* **72,** 231–242.
34. Leibiger, I. B., Leibiger, B., Moede, T. & Berggren, P. O. (1998) *Mol. Cell* **1,** 933–938.
35. Kulkarni, R. N., Bruning, J. C., Winnay, J. N., Postic, C., Magnuson, M. A. & Kahn, C. R. (1999) *Cell* **96,** 329–339.
36. Leibiger, B., Leibiger, I. B., Moede, T., Kemper, S., Kulkarni, R. N., Kahn, C. R., de Vargas, L. M. & Berggren, P. O. (2001) *Mol. Cell* **7,** 559–570.
37. Withers, D. J., Burks, D. J., Towery, H. H., Altamuro, S. L., Flint, C. L. & White, M. F. (1999) *Nat. Genet.* **23,** 32–40.
38. Kulkarni, R. N., Holzenberger, M., Shih, D. Q., Ozcan, U., Stoffel, M., Magnuson, M. A. & Kahn, C. R. (2002) *Nat. Genet.* **31,** 111–115.
39. Ding, V. W., Chen, R. H. & McCormick, F. (2000) *J. Biol. Chem.* **275,** 32475–32481.